



Toughening effect of Ni on nc-CrAlN/a-SiN_x hard nanocomposite

Yu Xi Wang^a, Sam Zhang^{a,*}, Jyh-Wei Lee^{b,c}, Wen Siang Lew^d, Bo Li^e

^a School of Mechanical and Aerospace Engineering, Nanyang Technological University, Singapore 639798, Singapore

^b Department of Materials Engineering, Ming Chi University of Technology, Taipei 24301, Taiwan

^c Center for Thin Film Technologies and Applications, Ming Chi University of Technology, Taipei 24301, Taiwan

^d School of Physical and Mathematical Sciences, Nanyang Technological University, Singapore 637371, Singapore

^e Central Iron and Steel Research Institute, Beijing 100081, China

ARTICLE INFO

Article history:

Received 7 July 2012

Received in revised form 2 November 2012

Accepted 6 November 2012

Available online 14 November 2012

Keywords:

Nanocomposite

Toughness

Nickel

Magnetron sputtering

ABSTRACT

To combat the brittleness of hard nc-CrAlN/a-SiN_x nanocomposite (nc-: nanocrystalline, a-: X-ray amorphous), different Ni content (from 0 to 39.8 at.%) is doped via magnetron sputtering. Glancing Angle X-ray Diffractometry, X-ray photoelectron spectroscopy, Field Emission Scanning Electron Microscopy and Transmission Electron Microscopy are employed to investigate the microstructural evolution. With increased Ni, the grain size decreases accompanied with morphology change, from dense glassy to coarse columns. With 4.2 at.% Ni, scratch toughness of nc-CrAlN/a-SiN_x hard nanocomposite (28 GPa) is improved by around 200% at expense of only 18% hardness.

© 2012 Elsevier B.V. All rights reserved.

1. Introduction

The initiative to develop nc-Me_nN/a-SiN_x nanocomposites (Me = W, V, Cr, Ti, Al, TiAl, CrAl, etc.; nc = nanocrystalline; a = X-ray amorphous) was to obtain enhanced hardness and wear resistance [1,2]. These improvements come from the segregated thin layer (i.e. a few monolayers) of a-SiN_x which prohibited the local sliding along grain and phase boundaries [3,4]. In addition to the growing strength, the durability of machining tools is more concerned in practical industrial applications and is usually realized by increasing fracture toughness. Therefore, it is increasingly desired for the super-hard nanocomposites if enhanced hardness can be complemented with proper toughness [3,5].

To authors' knowledge, however, quite few number of work are documented [6,7] on the toughening of nc-CrAlN/a-SiN_x, a state-of-the-art nanocomposite due to its superior oxidation resistance in addition to high strength [8]. Incorporation of ductile metallic phase is straightforward in increasing toughness as in the cases of crystalline nitrides and oxides embedded in Cu [9,10]. In this study, Ni is selected as toughening agent due to its great potential as illustrated in Ni doped TiN/SiN_x [11]. By increasing Ni from 0 to 39.8 at.%, the dependence of hardness and toughness on the microstructure evolution is revealed and an optimized fraction of Ni in balancing the hardness and toughness is achieved.

2. Experimental

Coating deposition was conducted via co-sputtering of Ni, Si and Cr_{0.7}Al_{0.3} targets in mixed Ar and N₂ ambient. Si (1 0 0) wafer and mirror-polishing stainless steel (SUS420C) discs were used as the substrates. All the substrates were subject to sequentially ultrasonic cleaning in acetone, ethanol and di-ionized water, followed by drying in N₂ atmosphere. Before deposition, the pressure of chamber was pumped better than 5 × 10⁻⁵ with outgassing for overnight. During deposition, the working pressure was maintained at 0.4 Pa. Flow rate of Ar and N₂ was controlled at 40 and 20 sccm, respectively. The substrate temperature was kept at 400 °C and the negative bias voltage was set at 160 V. The power density on the Cr_{0.7}Al_{0.3} and Si targets was set at 2.2 W/cm² and 4.1 W/cm², respectively. While that on the Ni target varied from 0.2 to 2.2 W/cm² to achieve different doping amounts. Detailed operating parameters are summarized in Table 1. It should be pointed out that the total thickness of all the coatings was controlled at around 2 μm.

The chemical compositions were evaluated using Field Emission Electron Probe Micro-Analyzer (FE-EPMA, JEOL JXA-8500F) with the aid of ZAF-corrected program. Crystalline structure was analyzed using Glancing Angle X-ray Diffractometry (GAXRD, Panalytical X'Pert Pro) with glancing incident of 1° at the scanning rate of 0.3° per 0.5 s. The bonding states were determined using X-ray photoelectron spectroscopy (XPS, Kratos AXIS Ultra) with a monochromatic Al Kα (1486.71 eV) X-ray radiation (15 kV/10 mA). To investigate the microstructure evolution, Field

* Corresponding author.

E-mail address: MSYZHANG@ntu.edu.sg (S. Zhang).

Table 1
Deposition parameters in fabricating Ni doped CrAlSiN coatings.

	CrAlSiN	CrAlSiNiN-1	CrAlSiNiN-2	CrAlSiNiN-3	CrAlSiNiN-4	CrAlSiNiN-5
Base pressure (Pa)				$<5 \times 10^{-5}$		
Working pressure (Pa)				0.4		
Ar:N ₂ gas ratio				2:1		
Total gas flow (sccm)				60		
Plasma etching ^a			15 min Ar ⁺ bombardment at 0.4 Pa at V _b = 160 V			
Substrate temperature (°C)				400		
Power density of Cr _{0.7} Al _{0.3} (W/cm ²)				2.2		
Power density of Si (W/cm ²)				4.1		
Power density of Ni (W/cm ²)	0	0.2	0.3	0.6	1.1	2.2
RF negative bias voltage (V)				160		
Coating thickness (nm)				2000		
Substrate			Si wafer (1 0 0) and SUS420C			

^a Plasma etching before deposition.

Emission Scanning Electron Microscopy (FESEM, JEOL JSM-6701F) and Transmission Electron Microscopy (TEM, JEOL JEM-2010F) were also employed.

Hardness was routinely determined via nanoindentation (Hysitron TI-900 Triboindenter) at the indent depth less than 1/10 of the coating thickness. Toughness evaluation, on the other hand, is still a challenging endeavor. To date, no universal technique or analysis approach is available to determine the toughness of thin films due to the size limitation [12]. In this study, Scratch Crack Resistance (CPR_s) [13] was used to benchmark the capability of preventing crack initiation and propagation. In short, the scratch tests were conducted using micro-scratch tester (J&L Tech. Scratch Tester) on the coatings deposited on SUS420C substrates. Linearly increased load from 0 to 50 N was applied when stylus moving along the coating surface (5 mm in length). The average value of lower (L_{c1}) and higher (L_{c2}) critical load were obtained from three scratches. The outcome of $L_{c1} \times (L_{c2} - L_{c1})$ gives rise to the index of toughness (i.e. CPR_s).

3. Results and discussion

3.1. Microstructure characterization

The chemical concentrations of Ni doped nc-CrAlN/a-SiN_x nanocomposites are listed in Table 2. Si retains at around 10 at.% as Ni varied from 0 to 23.4 at.%, but slightly decreases to 8.5 at.% when Ni is 39.8 at.%. Calculated Si/(Cr + Al) increases monotonically with the increase of Ni, indicating that Si atoms are more stable in this chemical condition. This is due to the smaller enthalpy of formation of the Si–N (–642.1 kJ/mol [14]) as compared to that of Al–N (–297 kJ/mol) and Cr–N (–117 kJ/mol) [15,16]. The oxygen which comes from the residual gas in the chamber maintains at around 1 at.% but spiking up to around 2 at.% when Ni content is increased to 39.8 at.%.

Fig. 1 demonstrates the dependence of crystalline structure on the Ni content. Without Ni, coatings are nc-CrAlN/a-SiN_x in the face-center-cubic (fcc) structure. This originates from the fact that Al replaces the Cr in fcc-CrN thus leads to the formation of solid-solution CrAlN. The formation of a-SiN_x is inferred from the results of our [6] and other researchers' previous studies [8], where ~10 at.% Si led to nc-CrAlN encapsulated by a-SiN_x. As Ni increases from 1.4 to 23.4 at.%, diffraction peaks shift toward higher position with peak broadening. Peak shifting comes from the lattice distortion since Ni atoms have chance to disperse in the CrAlN lattice and also from the formation of solid-solution CrAl(Ni)N, where Ni could possibly bond with Al to form AlNi or AlNi₃. The standard diffraction patterns of NiAl and Ni₃Al are referenced in Fig. 1 as well. However, it should be noted that Al prefers to bond with N since the enthalpy of formation of NiAl is in the rage between –59.8 and –72 kJ/mol and that of Ni₃Al is from –37.6 to –47.0 kJ/mol [17,18], less than

that of AlN (–297 kJ/mol). When Ni amount is 39.8 at.%, metallic Ni peaks become predominant as seen from the increased peak intensity of (1 1 1), (2 0 0) and (2 2 0) from fcc-Ni. Under this circumstance, excessive Ni agglomerate in a large amount thus suppresses the signal of other species (i.e. nc-CrAlN, AlNi and AlNi₃).

In addition to the peak shifting, peak broadening is also noticeable. This broadening is attributed to the reduced grain size. Studies of Ni doped TiN [19] and Ni doped nc-TiN/a-SiN_x [11] have revealed that Ni adatoms could form together with the a-SiN_x as an amorphous covering layer to block the grain growth. In this study, the calculated grain size decreases from ~7 to ~2 nm when Ni

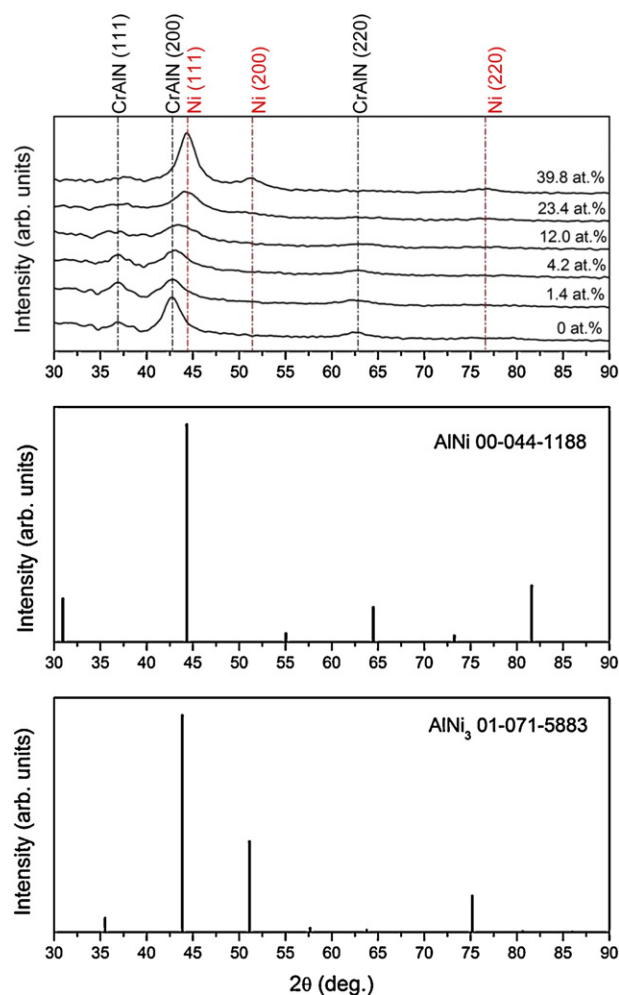


Fig. 1. GAXRD results of nc-CrAlN/a-SiN_x with different Ni content.

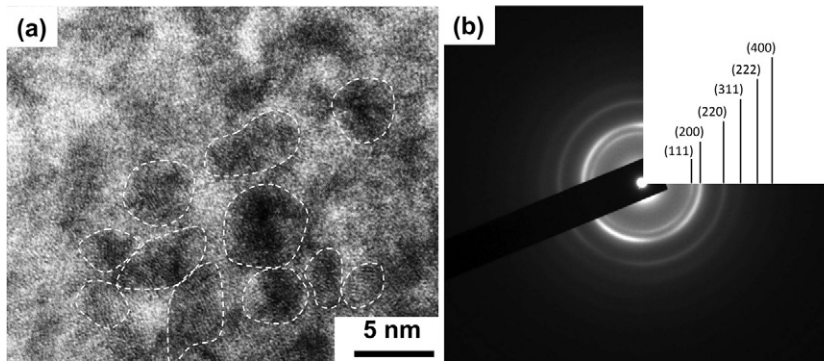


Fig. 2. TEM image (a) and corresponding selected area diffraction patterns (b) of nc-CrAlN/a-Si_x with 12.0 at.% Ni.

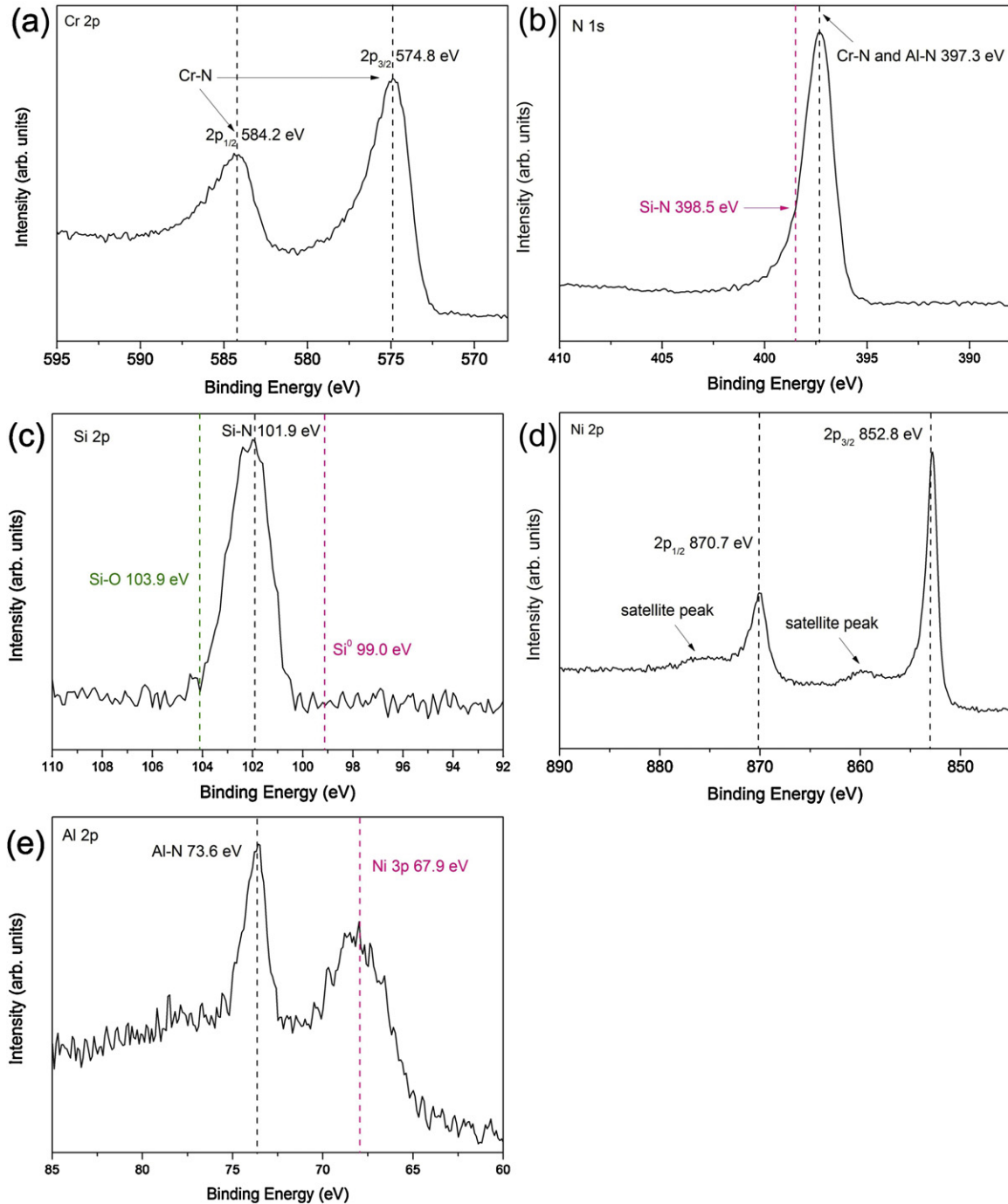


Fig. 3. XPS narrow scan of CrAlSiN with 12.0 at.% Ni: (a) Cr 2p, (b) N 1s, (c) Si 2p, (d) Ni 2p and (e) Al 2p.

Table 2
Summary of chemical concentration and grain size.

Coatings	Concentration (at.%)						Si/(Cr + Al)	Grain size (nm)
	Cr	Al	Si	N	Ni	O		
CrAlSiN	22.9	11.1	10.3	54.8	0	0.9	0.3	7
CrAlSiNiN-1	21.5	10.5	10.5	54.9	1.4	1.2	0.33	5
CrAlSiNiN-2	20.9	10.4	10.5	52.9	4.2	1.1	0.34	5
CrAlSiNiN-3	18.5	9.2	10.9	48.1	12.0	1.3	0.39	3
CrAlSiNiN-4	16.3	8.2	10.0	40.5	23.4	1.6	0.41	2
CrAlSiNiN-5	13.1	6.4	8.3	29.8	39.8	1.9	0.43	17

content increases to 23.4 at.% (Table 1). The mechanisms of generating nanocrystallites in nc-Me_nN/a-SiN_x have been discussed in great length in Ref. [20]. Previous studies of Ni doped TiN and TiSiN also showed that until its content reached up to around 50 at.%, Ni cannot crystallize [11,19]. In this study, metallic Ni dominates and becomes more crystallized when Ni content reaches to 39.8 at.%. In parallel, the calculated grain grows to 17 nm due to the Ni agglomeration.

Fig. 2(a) illustrates the high-resolution TEM image of nc-CrAlN/a-SiN_x with 12.0 at.% Ni. Nanocrystalline CrAlN (as circled) is observed in the scale of around 3 nm, in good agreement with the calculated value. These nano-grains embed in the amorphous phase as confirmed from the crystalline and the amorphous rings in the selected area diffraction patterns (Fig. 2(b)). Rings of (1 1 1) and (2 0 0) are evidentially observed, in correspondence with the results of XRD. With the aid of XPS, the bonding states in nanocomposite with 12.0 at.% Ni are revealed. Cr bonds with N as seen from the peaks centered at 584.2 and 574.8 eV (Fig. 3(a)). N bonding with Cr and Al is observed from N 1s narrow scan, in which N is also partially bonded with Si (Fig. 3(b)). Si–N bonding is confirmed from the Si 2p peak (Fig. 3(c)) centered at 101.9 eV. No pure Si (99.0 eV) or Si–O (103.9 eV) bonds can be observed, indicating Si entirely bond with N. In Ni 2p peak (Fig. 3(d)), binding energy of 852.8 eV (Ni 2p_{3/2}) and 870.7 eV (Ni 2p_{1/2}) are assigned to Ni⁰ state [11,21]. No other bonding state of Ni such as Ni²⁺ (854.6 eV) or Ni³⁺ (856.1 eV) can be observed. However, it is difficult to differentiate Ni–Al bonds due to the overlapped binding energy. Al 2p (Fig. 3(e)) centered at 73.6 indicates Al is bonded with N. The peak at the lower binding energy (67.9 eV) is from Ni 3p. Herein, Ni 3p peak is considered the synergetic contribution of pure Ni and Ni–Al bonds. However, it is unable to deconvolute this peak due to the binding energy overlapping. Fig. 4 exhibits the tendency of Ni 3p as a function of Ni content. With increased Ni, the peak intensity of Ni 3p and the intensity ratio of Ni/Al increase accordingly. When Ni increases from 1.4 to 23.4 at.%, no significant deviation in peak position can be observed. However when Ni is 39.8 at.%, Ni 3p peak shifts to a higher position. This shift is attributed to the formation of Ni–O due to the higher amount of oxygen involved (1.9 at.%).

An obvious change in morphology is revealed in Fig. 5. When Ni content is less than 12.0 at.%, dense glassy texture is observed. However, at 23.4 at.% Ni, columns perpendicular to the substrate emerge. At even higher Ni content (39.8 at.%), coarse columns become apparent. This evolution is attributed to the fact that with increased content, Ni agglomerates and grows into large grains.

3.2. Toughening effect of Ni

The dependence of hardness against scratch toughness of nanocomposite on the Ni content is presented in Fig. 6. Although grain size decreases, hardness suffers continuous drop from 27 to 12 GPa when Ni increases from 0 to 23.4 at.%. For nc-Me_nN/a-SiN_x nanocomposite, a threshold of amorphous fraction exists, beyond which drastic degradation takes place [3]. In the pure

nc-CrAlN/a-SiN_x nanocomposite, 10 at.% Si may already reach to this critical point. Therefore any addition of Ni (at small amount) would render excessive fraction of amorphous phase thus the hardness decreases. However, hardness declines to around 10 GPa (39.8 at.% Ni) is caused by the large crystallized grains of metallic Ni. Under this circumstance, large amount of Ni leads to the severe coarse columnar structure thus the degraded strength. Scratch toughness, on the other hand, increases continuously owing to the addition of Ni. As seen from the images of fracture behavior, increased critical load (*L*₂) and less chipping or buckling indicate tougher and more durable feature are achieved under contact force. This improvement originates from the ductile phase deformation thus blunting the crack tip so that more work is required for crack propagation.

Considering the practical use where hardness should be higher than 20 GPa, the optimized coating is the one with 4.2 at.% Ni.

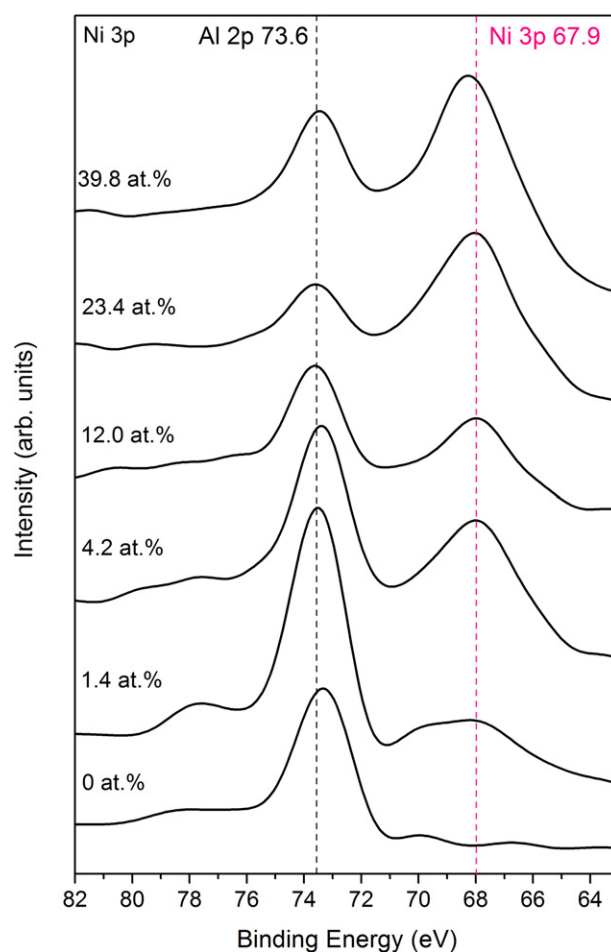


Fig. 4. Tendency of Al 2p and Ni 3p intensities as a function of Ni content.

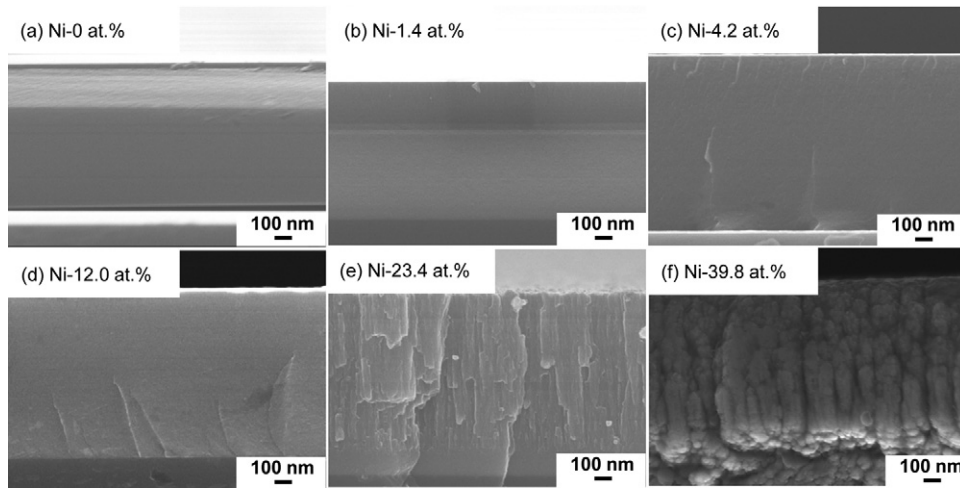


Fig. 5. Cross-sectional morphology of nc-CrAlN/a-SiN_x with different Ni content.

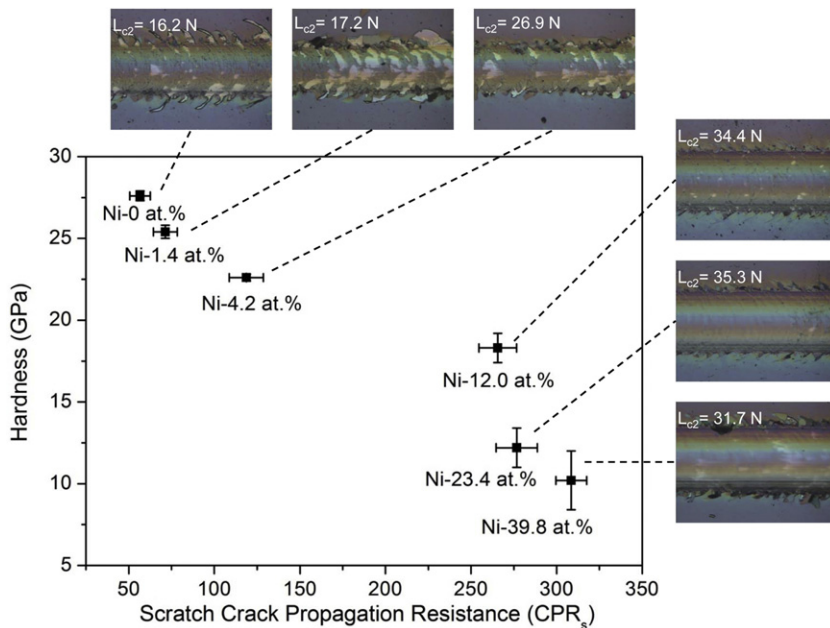


Fig. 6. Plot of hardness versus scratch toughness and fracture behavior after scratch of nc-CrAlN/a-SiN_x with varied Ni content.

In these coatings, scratch toughness of hard nc-CrAlN/a-SiN_x nanocomposite increases by around 200% at expense of only 18% hardness.

4. Conclusion

nc-CrAlN/a-SiN_x hard nanocomposites with varied Ni addition (from 0 to 39.8 at.%) have been synthesized via magnetron sputtering. With small amount of Ni (from 0 to 23.4 at.%), grain size decreases from 7 to 2 nm. However, further increase of Ni leads to the grain growth and coarse morphology. With proper amount of Ni (4.2 at.%), scratch toughness of pure nc-CrAlN/a-SiN_x nanocomposite (28 GPa) is improved by around 200% at expense of only 18% hardness.

Acknowledgement

This work is financially supported by the project AcRF Tier 2 (project code: T208A1218 ARC4/08), Singapore.

References

- [1] S. Veprek, S. Reiprich, *Thin Solid Films* 268 (1995) 64–71.
- [2] S. Veprek, M.J.G. Veprek-Heijman, *Surface and Coatings Technology* 202 (2008) 5063–5073.
- [3] S. Zhang, H.L. Wang, S.E. Ong, D. Sun, X.L. Bui, *Plasma Processes and Polymers* 4 (2007) 219–228.
- [4] A.D. Pogrebnjak, A.P. Shpak, N.A. Azarenkov, V.M. Beresnev, *Physics-Usppekhi* 52 (2009) 29–54.
- [5] S. Zhang, D. Sun, Y. Fu, H. Du, *Surface and Coatings Technology* 198 (2005) 2–8.
- [6] Y.X. Wang, S. Zhang, J.W. Lee, W.S. Lew, D. Sun, B. Li, *Surface and Coatings Technology* (2012), <http://dx.doi.org/10.1016/j.surfcoat.2012.03.036>.
- [7] Y.X. Wang, S. Zhang, J.-W. Lee, W.S. Lew, D. Sun, B. Li, *Nanoscience and Nanotechnology Letters* 4 (2012) 375–377.
- [8] H.-W. Chen, Y.-C. Chan, J.-W. Lee, J.-G. Duh, *Surface and Coatings Technology* 205 (2010) 1189–1194.
- [9] J.H. Hsieh, P.C. Liu, C. Li, M.K. Cheng, S.Y. Chang, *Surface and Coatings Technology* 202 (2008) 5530–5534.
- [10] M. Jirout, J. Musil, *Surface and Coatings Technology* 200 (2006) 6792–6800.
- [11] S. Zhang, D. Sun, Y. Fu, Y.T. Pei, J.T.M. De Hosson, *Surface and Coatings Technology* 200 (2005) 1530–1534.
- [12] S. Zhang, X. Zhang, *Thin Solid Films* 520 (2012) 2375–2389.
- [13] S. Zhang, D. Sun, Y. Fu, H. Du, *Thin Solid Films* 447–448 (2004) 462–467.

- [14] J. Soldan, J. Neidhardt, B. Sartory, R. Kaindl, R. Cerstvy, P.H. Mayrhofer, R. Tes-sadri, P. Polcik, M. Lechthaler, C. Mitterer, *Surface and Coatings Technology* 202 (2008) 3555–3562.
- [15] X.-Z. Ding, X.T. Zeng, Y.C. Liu, *Thin Solid Films* 519 (2011) 1894–1900.
- [16] K.P. Budna, P.H. Mayrhofer, J. Neidhardt, E. Hegedus, I. Kovacs, L. Toth, B. Pecz, C. Mitterer, *Surface and Coatings Technology* 202 (2008) 3088–3093.
- [17] Y. Wang, Z.K. Liu, L.Q. Chen, *Acta Materialia* 52 (2004) 2665–2671.
- [18] P. Nash, O. Kleppa, *Journal of Alloys and Compounds* 321 (2001) 228–231.
- [19] A. Akbari, J.P. Riviere, C. Templier, E. Le Bourhis, *Surface and Coatings Technol-ogy* 200 (2006) 6298–6302.
- [20] S. Veprek, M.G.J. Veprek-Heijman, *Surface and Coatings Technology* 201 (2007) 6064–6070.
- [21] A.P. Grosvenor, M.C. Biesinger, R.S.C. Smart, N.S. McIntyre, *Surface Science* 600 (2006) 1771–1779.